Synthetic Metals 161 (2011) 235–240

Contents lists available at ScienceDirect

Synthetic Metals

journal homepage: www.elsevier.com/locate/synmet

Reflective behavior of strong absorption metallic photonic crystals

Dengteng Ge[a], Lili Yang[b], Yao Li[a,*], Jiupeng Zhao[c], Xue Li[b], Huijie Zhao[d]

[a] Center for Composite Materials and Structures, Harbin Institute of Technology, Harbin 150080, PR China
[b] School of Transportation Science and Engineering, Harbin Institute of Technology, Harbin 150001, PR China
[c] School of Chemical Engineering, Harbin Institute of Technology, Harbin 150001, PR China
[d] Space Materials and Environment Engineering Laboratory, Harbin Institute of Technology, Harbin 150001, PR China

ARTICLE INFO

Article history:
Received 16 April 2010
Received in revised form
17 November 2010
Accepted 19 November 2010
Available online 6 January 2011

Keywords:
Metallic photonic crystals
Absorption
Effective fraction
Windows

ABSTRACT

The growing interest in fabrication and investigation of metallic photonic crystals is determined by the potential for new properties and applications. In this work, reflective spectra of strong absorption metallic photonic crystals including metal/template composites and metalic inverse opals were systematically studied. Fe–Ni alloy were electrodeposited through self-assembly templates, and inverse opals were fabricated after removal of templates. For metal/template composites, enhanced stop gap is blue shifted due to strong absorption of metallic materials. An effective fraction of alloy is introduced for the first time to describe the alloy participating in the Bragg effect, which is mainly determined by metal. However, alloy inverse opals show greater blue shift of broaden gap to high frequency regions and metallic nature in low frequency regions due to the existence of windows. Scanning electronic micrographs results indicate that there is a critical thickness of wall materials where there are windows in inverse opals. It is proposed here that windows are formed due to the associated breaking of thin alloy walls with template.

1. Introduction

Metallic photonic crystals (PhC) have attracted considerable attention due to their potential applications in high-efficiency light sources [1], chemical detection [2], optoelectronic and biophotonic devices [3] as well as battery electrode [4]. Since the first example of metallic inverse opal structures reported by Jiang [5] and Velev et al. [6], various metals, especially strong absorption metals, for example, Au, Ag, W [7], Ni [8,9], Ge [10] have been fomed into inverse opals. Some interesting results were found for the reflective behavior of metallic PhC. For example, the reflectance was found greatly enhanced after the silver infiltration [11] or after the deposition of tungsten for metal/template PhC [7]. It is summarized that these interesting optical properties are exhibited including thermally stimulated emission behavior [12] and plasmonic physics [13] because of the interplay between electronic plasma screening effects and geometrical scattering effects [14,15]. P.N. Bartlett [3] and Paul V. Braun [16] studied the reflective behavior of metallic inverse opals using a monolayer template as a function of film thickness and with the control of structural openness, respectively, However, the absorpting light in metallic materials was not taken into consideration. In this research, we demonstrate electrochemical deposited PhC of strong absorption Fe–Ni alloy, including alloy/template PhC and alloy inverse opals from polystyrene (PS) templates. Their reflective behaviors were discussed and found to be associated with an effective fraction of metallic materials in strong absorption metal/PS and windows in metallic inverse opals.

2. Experimental

2.1. Fabrication of PS opals

Monodispersed PS spheres (diameters 325, 400 and 525 nm) were obtained by using an emulsifier-free emulsion polymerization technique. Indium tin oxides (ITO) glass slides were used as the substrates for PS template growth. PS colloidal crystals were grown by using a controlled vertical drying method [17]. ITO glass substrates were placed into cylindrical vessels vertically. Then PS dispersion with a concentration of 0.1% added into the vessels and dried in an incubator at a stable temperature of 60 °C. After water slowly evaporated, well ordered templates are robust and adhere well to the substrates and appear distinct colors.

2.2. Electrodeposition preparation of Fe–Ni alloy/PS and alloy inverse opals

Electrolyte was prepared by dissolving chemical reagents following nickel sulfate, ferric sulfate, sodium chloride, boracic acid

* Corresponding author. Tel.: +86 451 86402345; fax: +86 451 86402345.
E-mail address: liyao@hit.edu.cn (Y. Li).

0379-6779/$ – see front matter © 2010 Elsevier B.V. All rights reserved.
doi:10.1016/j.synthmet.2010.11.025

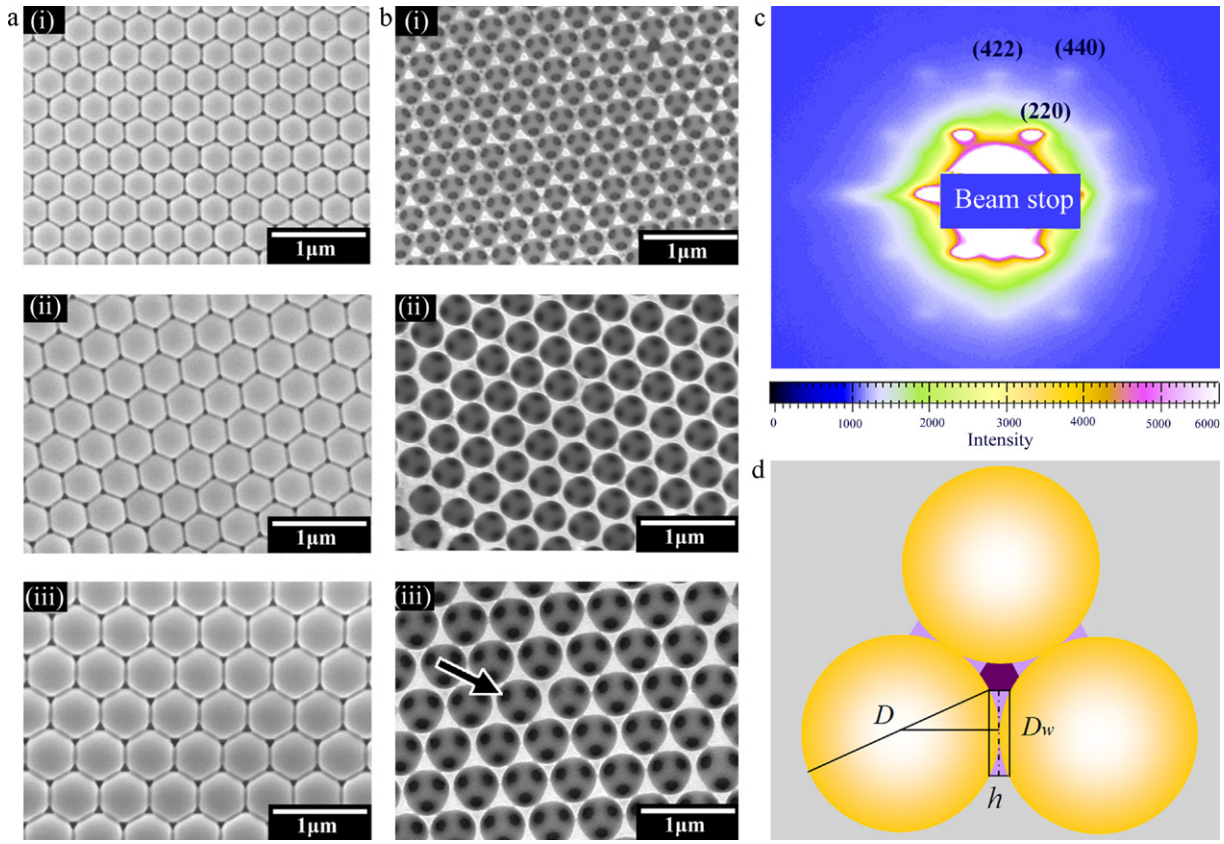

Fig. 1. (a) Top-viewed SEM images of Fe–Ni alloy/PS PhC from different sizes of PS spheres. (b) Top-viewed SEM images of corresponding alloy inverse opals. (c) SAXS pattern of Fe–Ni alloy/PS PhC with 330 nm of PS spheres. (d) A schematic illustration of cross-sectional alloy inverse opals.

and SDS in ultrapure water. The concentrations of plating solutions were described in many articles [16]. Pure Ni and ITO glass coating with PS opal photonic crystals ere used as anode and cathode, respectively. After installed the electrodes, electrodepositing was carried out under a current density of 3.0 A/dm^2 for 4 min at the condition of 50–60 °C and pH = 3–4. The content of Fe and Ni was controlled as 1:4 by the ratio of iron to nickel ion in the electrolyte solution. The alloy inverse opals were obtained after the removal of templates by dissolution in tetrahydrofuran (THF) for 24 h. Furthermore, in order to understand the effect of PhC structure on the optical properties, Fe–Ni alloy film was also prepared on ITO glass without PS templates under the same electrodeposition conditions.

2.3. Characterizations

Samples were coated with platinum and observed using MX260FE scanning electron microscopy (SEM) (Camscan Corp., England) at an accelerating voltage of 20 kV. The reflection spectra were obtained from PE Lambda 950 UV–Vis–NIR spectrometer (the beam spot was 5 mm × 5 mm in area). The incident light was oriented 8° deviation from perpendicular to the surface of samples. Small angle X-ray scattering (SAXS) experiments were performed at 1W2A beamline at Beijing Synchrotron Radiation Facility, China. A two dimension charge-coupled detector (CCD) camera with diameter of 165 mm and pixel size of 80 μm × 80 μm was used and the distance between CCD and sample was 4.85 m.

3. Results

3.1. Morphologies of Fe–Ni alloy PhC

Top-viewed SEM micrographs of alloy/PS PhC (Fig. 1a) reveal good ordering close packed arrays of PS templates with domain size. This is indicative of the deposition of Fe–Ni alloy between the interspaces of PS beneath the out layer. The center-to-center distance of PS spheres D are obtained 330, 410, 530 nm through direct measurement, respectively. To evaluate the ordered structure over the whole sample, SAXS pattern of alloy/PS PhC with size of 330 nm is shown in Fig. 1c. The sharp Bragg speckles suggests that a single-crystal domain of fcc structure is irradiated by the X-ray beam. Through the comparison of scattering speckles' distance from center of scattering, the scattering pattern can be indexed. For an fcc lattice q values of each crystalline diffraction plane (q_{hkl}) are calculated from [18]:

$$q = \frac{2\pi}{d_{hkl}} = \frac{\sqrt{2}\pi}{D}\sqrt{(h^2 + k^2 + l^2)} \quad (1)$$

where d_{hkl} is the interplanar spacing between ($h\,k\,l$) planes. Then D can be calculated to be 310 nm, which is very little smaller than the SEM value. It may be because the evaporation of platinum increases the real distance of spheres. After the removal of PS templates, macropores are formed and the top-viewed alloy inverse opals were shown bowl-like (Fig. 1b). The dark zone marked by arrows is called "window" through which macropores are interconnected. It has been reported that windows are might formed due to the shrinkage of templates [19], the reason of which has

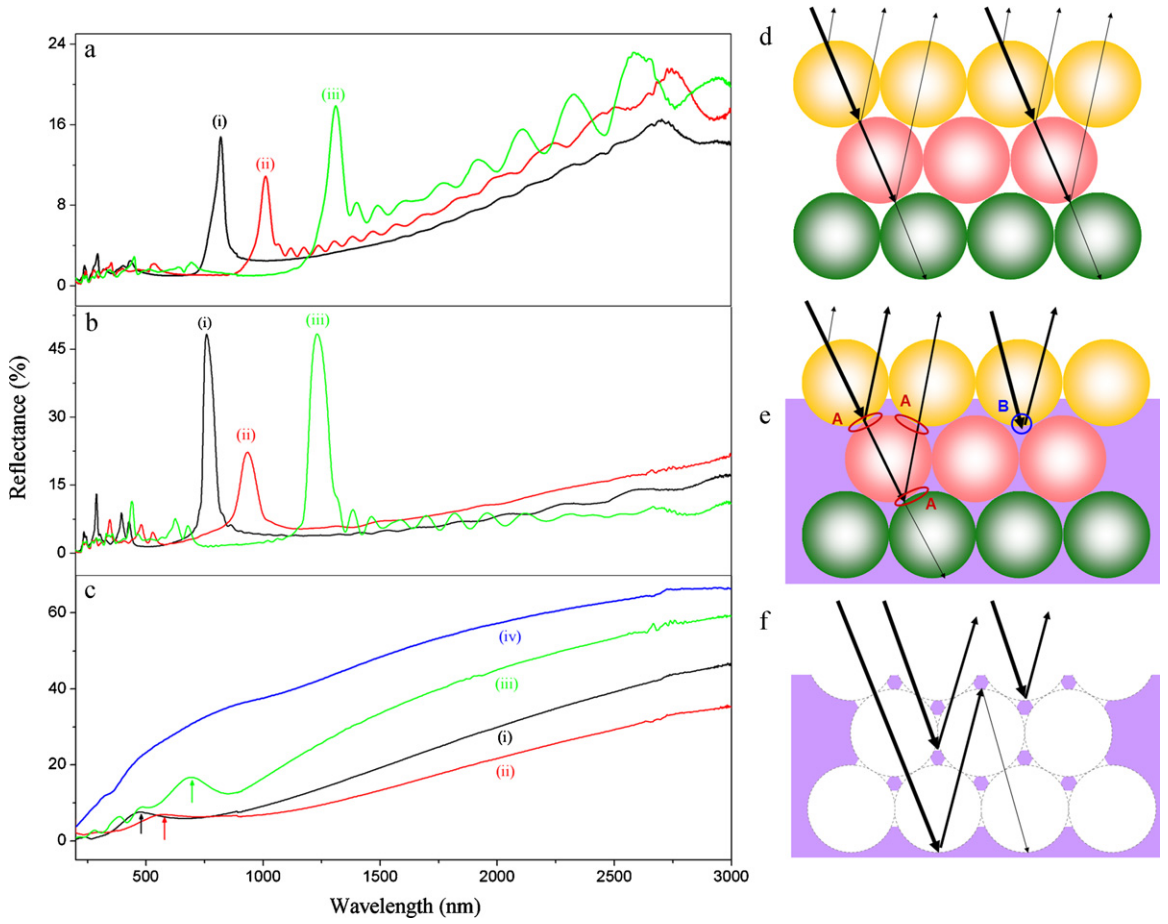

Fig. 2. (a) Reflectance from three kinds of PS opals with size of 330 nm (i), 420 nm (ii) and 530 nm (iii). (b) Reflectance of Fe–Ni alloy/PS PhC. (c) Reflectance of Fe–Ni alloy inverse opals and electrodeposited alloy film without template (iv). More, schematic illustrations of ray paths on the surface of PS opals (d), Fe–Ni alloy/PS PhC (e) and Fe–Ni alloy inverse opals (f).

been unknown yet. Here we suppose that close-packed spheres do not shrinkage and are not overlapped. From the maximum width of dark zone in Fig. 1b, the diameter of window D_{window} can be measured and gives 112 nm, 125 nm and 150 nm, respectively. Thus, in the schematic diagram of Fig. 1d, the width of window h_{window} can be calculated easily from:

$$h_{window} = D - (D^2 - D_{window}{}^2)^{1/2} \quad (2)$$

It is interestingly found that the widths are obtained 19.6 nm, 19.8 nm and 21.7 nm, which are all close to 20 nm. Therefore it can be deduced that windows appear not due to the shrinkage of template, or else the diameter/width of windows is proportional to the size of sphere. Here 20 nm can be thought as a critical thickness of skeletal walls. During the removal of templates in THF solution, the wall lower than this critical thickness cannot undertake the stress caused by dissolution of PS and is prone to be broken. It is demonstrated the windows were formed due to the thin walls' broken during PS spheres' removal process. This is important for the understanding of structures of inverse opals.

3.2. Reflective behavior of PhC

In Vis–NIR region, the metallic materials exhibit high absorption, so the metallic PhC will likely have optical properties only in reflectance mode, not in the transmission mode [20]. Here reflectance spectrum of PS opals, alloy/PS PhC and inverse opals were tested using an UV–Vis–NIR spectrometer (Fig. 2a–c). Both PS opals and alloy/PS PhC show a pronounced (1 1 1) reflectance peak and several multilevel reflectance peaks. The position of gap occurs at λ_{max} = 820, 1012 and 1312 nm for opals while little blue shifted to 760 nm, 936 nm and 1232 nm after the infiltration of alloys.

This is very interesting because the average refractive index of PhC seems to increase due to the insertion of metallic materials. In Refs. [11,15], the position was also little red shifted after the infiltration of silver or tungsten. Moreover, the (1 1 1) diffraction intensity is greatly enhanced twice to thrice after the electrodeposition of alloy. For alloy inverse opals, the reflectance spectrum exhibit so different. Broaden Bragg peak in short wavelength region and metallic character in long wavelength region are shown. Yu et al. have proved that the reflectance performance of metallic inverse opals depends on their surface termination [16].

4. Discussion

4.1. Reflective behaviors of opals

All opals reveal pronounced reflectance peaks arising from the destructive interference effect between reflections off the layers of ordered structure (Fig. 2d). According to the Bragg's law, this peak results from the first order interference of (1 1 1) plane of fcc structure. Through Bragg–Snell's law, it can be calculated from:

$$\lambda_{max} = 2d \cdot (n_{eff}^2 - \sin^2 \theta)^{1/2} \quad (3)$$

$$n_{eff} = n_{sphere} f_{sphere} + n_{fill} f_{fill} \quad (4)$$

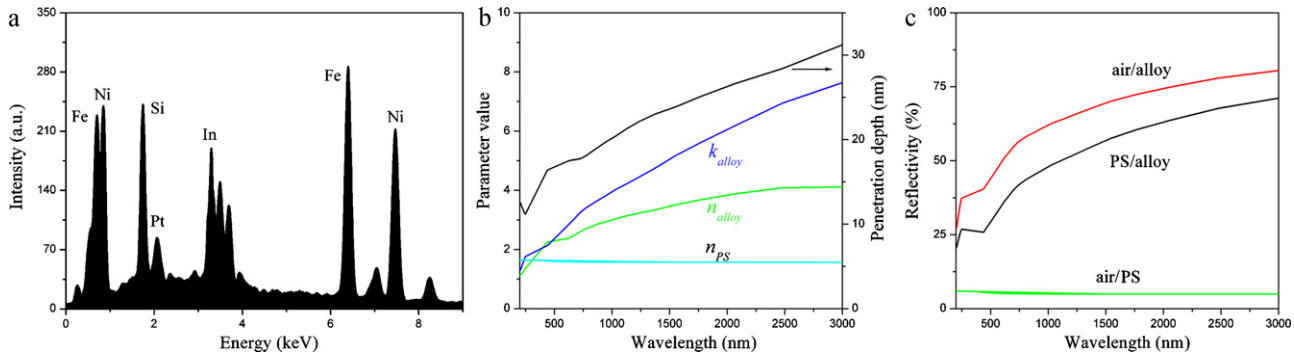

Fig. 3. (a) EDS data of Fe–Ni alloy inverse opal. (b) Refractive index n and extinction coefficient k of PS materials and alloy and also the penetration depth of alloy. (c) Reflectivity of lights at the air/alloy, PS/alloy and air/PS interfaces.

where d, n, θ and f are the interplanar spacing, refractive index of materials, the incidence angle against the normal film and each volume ratio, respectively. For PS opals, $n_{sphere} = 1.59$, $f_{sphere} = 0.746$, $n_{fill} = n_{air} = 1$ and $f_{fill} = 0.254$. In our tests $\theta = 8^{\circ}$, and for (1 1 1) plane there is $d = 0.816D$. The diameters of spheres are calculated 350 nm, 430 nm and 560 nm, which are very close to the observed experimental results. This means the Bragg–Snell's law is valid for PhC of PS materials.

4.2. Reflective behavior of alloy/PS PhC

The reflective behavior of metallic PhC is in essence related with the interaction between lights and materials. The interaction can be described by the material's dielectric constant (including refractive n and extinction coefficient k) and there are mainly three behaviors, i.e. transmission, absorption and reflection. The dielectric constants of Fe–Ni alloy can be obtained through parameters of bulk iron and nickel [21] from:

$$\begin{aligned} n_{alloy} &= n_{Fe} \cdot \nu_{Fe} + n_{Ni} \cdot \nu_{Ni} \\ k_{alloy} &= k_{Fe} \cdot \nu_{Fe} + k_{Ni} \cdot \nu_{Ni} \end{aligned} \tag{5}$$

where ν stands for the atomic fraction of iron or nickel within alloy materials. It is obtained $\nu_{Fe} = 0.48$ and $\nu_{Ni} = 0.52$ through the EDS data (Fig. 3a). The transmission and absorption behaviors can be evaluated by the penetration depth of light δ through materials. It can be calculated as [22]:

$$\delta = \frac{1}{\alpha} = \frac{\lambda}{4\pi \cdot k} \tag{6}$$

where λ is the incidence light wavelength. Thus, the penetration depth in PS spheres is considered to be infinitely large due to its extinction coefficient k access to zero. Fig. 3b also shows the calculated penetration depth of alloy materials. It is obvious that lights just penetrate into Fe–Ni alloy lower than few ten nanometers. The reflectivity of lights is another parameter for the dielectric performance of materials. As well known, the vertical reflectivity of lights at an interface from one dielectric material to another is approximately described as [23]:

$$R = \frac{(n_1 - n_2)^2 + (k_1 - k_2)^2}{(n_1 + n_2)^2 + (k_1 + k_2)^2} \tag{7}$$

Through the interface of air/PS, most of lights penetrate into PS materials while a few of lights are directly reflected (Fig. 3c). However, for both PS/alloy and air/alloy interfaces, most of lights are directly reflected and leftover lights are absorbed through alloy skeletal walls. Thus, strong absorption metals have this property of high reflection and opaqueness of lights, which is different from PS materials. The reflective behavior of opals, especially the alloy/PS PhC and metallic inverse opals as a function of wavelength will be associated with these results.

Fig. 2e shows the ray paths of parallel incident lights illuminating on alloy/PS PhC. Higher reflectivity happens and the reflections off the curved surfaces are greatly increased intrinsically. Hence the (1 1 1) diffraction intensity of first order is greatly enhanced. Lights can transmit through thin alloy walls like region *A*, however just reflection and absorption happen for thicker walls such as region *B*. It is deduced that just part of alloy materials are participating in the Bragg interference. We define the effective fraction of alloy φ_{trans}, then Eq. (4) is transformed into:

$$n_{eff} = n_{sphere} \cdot f_{sphere} + n_{alloy} \cdot f_{alloy} \cdot \varphi_{trans} \tag{8}$$

Through the experimental λ_{max} values and Eq. (3), the effective fraction φ_{trans} can be obtained 25.7%, 24.8% and 26%, respectively. It means that about a quarter of alloy can be treated as transmission medium of lights and participates in the Bragg effects while three quarters can be treated as the "black-hole" of lights. The effective fraction of alloy is introduced here statistically to reflect the absorption effect. Thus, in strong absorption metal/template PhC there is an effective fraction of metallic materials φ_{trans} for Bragg diffraction which is related with their dielectric property. Furthermore, if there is $n_{metal} \cdot \varphi_{trans} < 1$, the position of gap will be blue shifted, while $n_{metal} \cdot \varphi_{trans} > 1$ provided, the gap wavelength will be red shifted.

4.3. Reflective behavior of alloy inverse opals

From the 3D structure of inverse opals (Fig. 2f), it is indicated that thin alloy walls for diffraction and propagation of lights are decreased greatly due to the appearance of windows. Thus upper alloy within inverse opals acts as perfect mirrors while lower alloy acts as a black hole to suck lights. Therefore, the optical performance of metallic inverse opals is determined by the scale of upper few layers. The paths of lights in inverse opals can be deduced and shown in Fig. 2f. There are two effects windows bring to the interaction between PhC and lights. Firstly, compared with opals or alloy/PS composites, 3D ordered windows in inverse opals increase the sorts of ordered structures. When the incidence wavelength is small, destructive interference happens between reflective off the ordered skeletal walls rather than the refractions. The coupling of these ordered structures complicates the reflectance spectrum and broadens the reflection peak. Secondly, the penetration depth of lights is decreased due to the presence of windows. From Eq. (3), it can be concluded that the interplanar distance in Bragg effect is decreased due to the limited penetration depth of lights. When the incident wavelength is big, the optical path difference between reflective lights becomes so great that the Bragg law can not be satisfied due to the limited interplanar distance. Alloy inverse opals can be considered as porous metal films with rough surfaces in this case. Thus inverse opals reveal metallic and their optical properties can be explained from effective medium theory (EMT). This

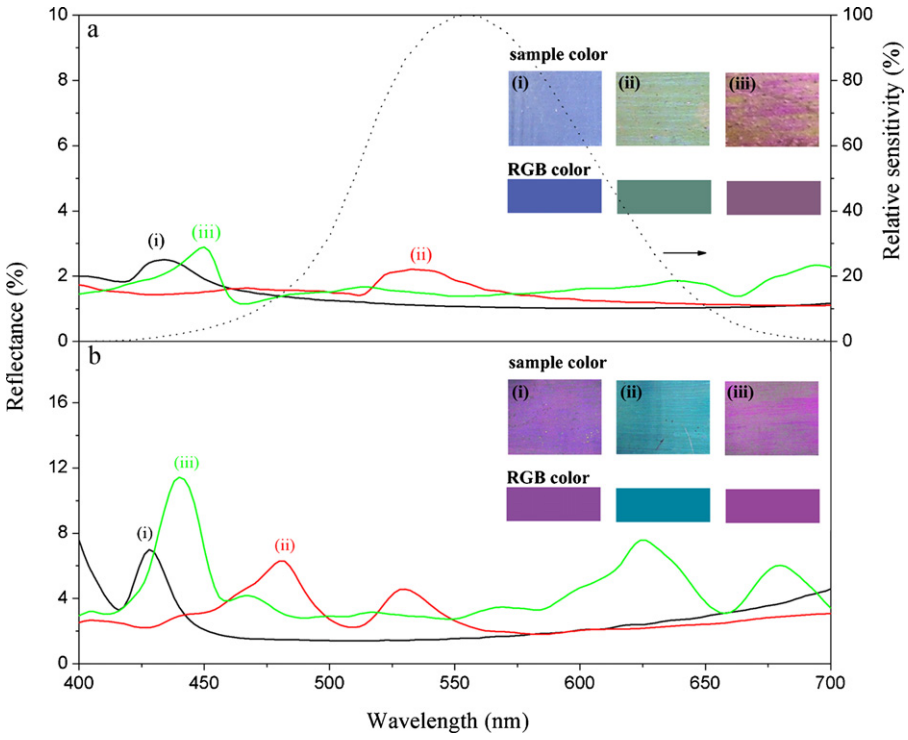

Fig. 4. (a) Human eyes' relative sensitivity curve (dotted line) in 400–700 nm region; reflectance spectrum as well as corresponding surface appearance of PS templates with size of 320 nm (i), 430 nm (ii), and 550 nm (iii). (b) Pictures of alloy/PS PhC and their reflectance spectrum in 400–700 nm.

can be easily proved from the similarity between the reflectance spectrum of inverse opals and that of electrodeposited Fe–Ni alloy film (Fig. 2c). It is deduced that metallic inverse opals with windows have structures defined on the scale of a few layers and the existence of windows may results in a redistribution of destructive interference energy.

4.4. Chromatic analysis

Both PS opals and Fe–Ni alloy/PS PhC are shown distinct colors (Fig. 4a and b) while alloy inverse opals are dark metallic through naked-eyes. As well known, the human eyes have high sensitivity with lights of wavelength in 400–700 nm region (Fig. 4a) [24]. In the 1931 CIE-XYZ standard chromatic system, the CIE-XYZ tristimulus chromatic values of each sample can be obtained from its reflectance spectrum during 400–700 nm [25]. Then the CIE-RGB chromaticity coordinates of each sample can be easily obtained after a conversion The theoretical color will be shown after a mixture of R, G and B, which are almost the same as the observed colors. This theoretically prove that the color of PhC is due to the multi diffraction peaks during 400–700 nm, which is different from that PhC with smaller size is mainly due to the first diffraction peaks [26]. Moreover, the colors of inverse alloy opals are generally similar with that of alloy films just because the reflection of alloy films is so strong.

5. Conclusions

In summary, we have reported systematic studies of reflectance spectrum of electrodeposited Fe–Ni alloy/PS PhC and alloy inverse opals. An effective fraction was introduced for strong absorption metallic materials. Greatly intensive peak are found for Fe–Ni alloy/PS PhC due to the perfect metallic reflectors and the position of gap is little blue shifted because of just a quarter of alloy involved in Bragg effect. For alloy inverse opals, the position of gap is significantly blue shifted to high frequency region owing to the existence of windows while metallic performance is shown in low frequency region. It was also proved that windows in inverse opals appear due to the associated breaking of narrow alloy walls with PS template and the critical thickness of alloy wall is about 20 nm. It is demonstrated that strong absorption metallic skeletal materials in the 3D ordered structures play a double-sided role of active perfect reflector and passive "black-hole" of lights. These results about the metallic photonic crystals are indeed helpful for better understanding their optical performance and provide facile method for photonic applications.

Acknowledgements

The authors gratefully acknowledge Prof. Zhonghua Wu and his team for their help in carrying out the SAXS experiments at Institute of High Energy Physics, Chinese Academy of Sciences, Beijing, China. This work is supported by the National Natural Science Foundation of China (20601006), Program for New Century Excellent Talents in University (CET2006), China Aerospace Science & Technology Corporation Innovation Foundation (CASC200906) and National Postdoctor Fundation (20100471033).

References

[1] I. Puscasu, M. Pralle, M. Mcneal, J. Daly, A. Greenwald, E. Johnson, R. Biswas, C.G. Ding, J. Appl. Phys. 98 (2005) 013531.
[2] M.I. Baraton, L. Merhari, Synth. React. Inorg. Met. Org. Chem. 3 (2005) 733.
[3] P.N. Bartlett, J.J. Baumberg, S. Coyle, M.E. Abdelsalam, Faraday Discuss. 125 (2004) 130.
[4] J. Banhart, Prog. Mater. Sci. 46 (2001) 559.
[5] J.G. Fleming, S.Y. Lin, I. El-Kady, et al., Nature 417 (2002) 52.
[6] E. Ozbay, Science 311 (2006) 189.
[7] A. Moroz, Phys. Rev. Lett. 83 (1999) 5274.
[8] I. El-Kady, M.M. Sigalas, R. Biswas, K.M. Ho, C.M. Soukoulis, Phys. Rev. B 62 (2000) 15299.
[9] P. Jiang, J. Cizeron, J.F. Bertone, V.L. Colvin, J. Am. Chem. Soc. 121 (1999) 7957.
[10] O.D. Velev, P.M. Tessier, A.M. Lenhoff, E.W. Kaler, Nature 401 (1999) 548.
[11] G. von Freymann, S. John, M. Schulz-Dobrick, E. Vekris, N. Ttreault, S. Wong, V. Kitaev, G.A. Ozin, Appl. Phys. Lett. 84 (2004) 224.

[12] L.B. Xu, W.L. Zhou, C. Frommen, R.H. Baughman, A.A. Zakhidov, L. Malkinski, J.Q. Wang, J.B. Wiley, Chem. Commun. 997–998 (2000) 997.
[13] P.N. Bartlett, M.A. Ghanem, I.S. El Hallag, P. de Groot, A. Zhukov, J. Mater. Chem. 13 (2003) 2596.
[14] X.D. Meng, R. Al-Salman, J.P. Zhao, N. Borissenko, Y. Li, F. Endres, Angewandte 48 (2009) 1.
[15] N. Pérez, A. Hüls, D. Puente, W. González-Vias, E. Castano, S.M. Olaizola, Sens. Actuators B 126 (2007) 88.
[16] X.D. Yu, Y.J. Lee, R. Furstenberg, J.O. White, P.V. Braun, Adv. Mater. 19 (2007) 1689–1692.
[17] M.A. Mclachlan, N.P. Johnson, R.M. Rue La De, D.W. McComb, J. Mater. Chem. 14 (2004) 144–150.
[18] S.S. Hu, Y.F. Men, S.V. Roth, R. Gehrke, J. Rieger, Langmuir 24 (2008) 1620.
[19] A. Stein, F. Li, N.R. Denny, Chem. Mater. 20 (2008) 650.
[20] M. Sigalas, C. Chan, K. Ho, C. Soukoulis, Phys. Rev. B 52 (1995) 11744.
[21] (a) P.B. Johnson, R.W. Christy, Phys. Rev. B 9 (12) (1974) 5060;
(b) E.D. Palik, Handbook of Optical Constants of Solids, Academic Press Inc., 1985.
[22] G. Bekefi, A.H. Barrett, Electromagnetic Vibrations, Waves and Radiation, MIT Press, 1977.
[23] C. Kisstle, Introduction to Solid State Physics, 8th ed., Wiley, New York, 2004.
[24] E.F. Schubert, Light Emitting Diodes, 2nd ed., Cambridge University Press, 2006.
[25] T. Smith, J. Guild, Trans. Opt. Soc. 33 (1931) 96–99.
[26] H. Fudouzi, Y. Xia, Langmuir 19 (2003) 9656.